Check for updates

Received: 21 October 2025 | Revised: 26 August 2026 | Accepted: 28 August 2026

DOI: 10.1002/qj.70311

Quarterly Journal of the Royal Meteorological Society RMetS

RESEARCH ARTICLE

A synoptic overview of the EUREC^{4}A field campaign

Leo Saffin[1,2,3] | Richard Jones[4] | Juliane Schwendike[2] | Arlene Laing[5] | Kathy-Ann Caesar[6] | Lyndon Alves[7,8] | Andre Charles[9] | Letitia Humphreys[10] | Carolyn Peck[11] | Cecile Marie-Luce[12,13] | Gregory Cato[14] | Nicola Alexander[6] | Elmo Burke[15] | Avlon Charlery[6] | Shamal Clarke[16] | Sheryl Etienne-Leblanc[17] | Carshena Gordon[17] | Danielle Nurse[18] | Kiran Sedoo[19] | Kaylinda Ward-Forbes[20] | Anton Wiltshire[19,21] | Shanea Young[22] | Leif Denby[2,23] | Douglas J. Parker[2,24] | Lorenzo Tomassini[3,25] | Alan Blyth[26] | Gary Lloyd[27] | Alexander G. Jong[28]

Correspondence
Leo Saffin, Department of Meteorology, University of Reading, Reading, UK.
Email: l.saffin@reading.ac.uk

Funding information
Natural Environment Research Council, Grant/Award Numbers: NE/S015752/1, NE/S015779/1; Caribbean Institute for Meteorology and Hydrology; World Meteorological Organization

Abstract

We present an overview of the important synoptic features that occurred during the EUREC^{4}A field campaign. These results are based on workshops bringing together forecasters and researchers to look in detail at cloud patterns in the region of interest (Barbados and the upstream trade winds) and how they were influenced by synoptic features. Consistent with previous studies, we found that the influence of, or lack of, midlatitude and subtropical features was important for cloud patterns. The strength and position of subtropical high-pressure systems strongly varied through the field campaign and could be linked to differences in cloud patterns as well as the transport of dry and dusty air from West Africa. Development of deeper clouds and more organised patterns typically coincided with an upper-level potential vorticity streamer associated with anticyclonic Rossby-wave breaking. The local Hadley circulation shows a strong climatological subsidence in the region of interest but had a positive anomaly for ascent during the field campaign, indicating favourable conditions for cloud development, albeit with substantial day-to-day variability. There was often much more detail in cloud patterns in any given satellite image than can be conveyed in a summary. Two features of note were a flowers cloud pattern along the boundary of dry and dusty air without dominating the region, and fish cloud patterns could be embedded within other types of cloud pattern with no associated front or shear line.

KEYWORDS

Barbados, cloud patterns, cumulus, EUREC^{4}A, fish, flowers, gravel, shallow convection, sugar, trade wind

For affiliations refer to page 16

This is an open access article under the terms of the Creative Commons Attribution License, which permits use, distribution and reproduction in any medium, provided the original work is properly cited.
© 2026 The Author(s). *Quarterly Journal of the Royal Meteorological Society* published by John Wiley & Sons Ltd on behalf of Royal Meteorological Society.

1 | INTRODUCTION

The Elucidating the Role of Cloud-Circulation Coupling in Climate (EUREC^{4}A) field campaign in January–February 2020 focused on observing shallow cumulus clouds in the trade-wind region upstream of the Caribbean—in particular Barbados and the surrounding environment—to better understand how cloud organisation is related to the large-scale environment (Stevens *et al.*, 2021). During the EUREC^{4}A field campaign, a novel set of in-situ observations was collected from instrumented unmanned aerial vehicle, aircraft flights, radiosonde and dropsonde launches, research vessels, and ground sites.

The response of trade-wind cumulus clouds to climate change has been shown to be highly uncertain in climate models; some models predict little change in trade-wind cumulus cloud cover, whereas others predict a strong reduction leading to reduced reflection of solar radiation and accelerated warming (Bony & Dufresne, 2005; Vial *et al.*, 2013; Zelinka *et al.*, 2020). A major motivation behind EUREC^{4}A was the large uncertainty in trade-wind cumulus cloud feedbacks in climate models and its contribution to climate sensitivity (Bony *et al.*, 2017). One of the aims of EUREC^{4}A was to provide a reference dataset that can be used as a benchmark for advancing the modelling and the satellite remote sensing of clouds and circulation, in addition to getting a better understanding of cloud–circulation coupling processes (Bony *et al.*, 2017).

The variability in trade-wind cumulus cloud cover is strongly linked to the mesoscale organisation of clouds. Prior to the EUREC^{4}A field campaign, a group of experts manually identified cloud patterns in satellite images and categorised four distinct patterns seen in trade-wind cumulus—sugar, gravel, fish, and flowers (Stevens *et al.*, 2020)—and showed that these cloud patterns are related to the large-scale environment (Bony *et al.*, 2020). More objective and automated methods have been used to identify a large distribution of different cloud patterns (Denby, 2020), and the four named patterns have been shown to be the extremes of a continuous distribution (Janssens *et al.*, 2021). Despite these limitations, the four categories of cloud patterns are useful for describing different time periods and giving an overview of the cloud organisation; for example, the Common Consensus on Convective Organization during the EUREC^{4}A Experiment (C^{3}ONTEXT) dataset of cloud patterns during EUREC^{4}A (Schulz, 2022).

A key result from EUREC^{4}A is that the observations ruled out the mechanisms of cloud feedback leading to stronger climate sensitivity in models (Vogel *et al.*, 2022). Vogel *et al.* (2022) showed that the mesoscale motion was the key controlling factor for cloud-base mass flux, rather than the thermodynamics. George *et al.* (2023) showed that shallow mesoscale overturning circulations are a common feature in the trade-wind region, as seen in the convergence and divergence calculated from dropsonde circles during EUREC^{4}A. These observations are consistent with the proposed mechanism for forming mesoscale organisation derived from large-eddy simulations: simulations have been shown to form organisation of trade-wind cumulus clouds through mesoscale circulations associated with shallow convection, which acts to converge moisture in already moist regions (Bretherton & Blossey, 2017; Janssens *et al.*, 2022). This mechanism has been reproduced in a simulation of the formation of the flowers pattern from EUREC^{4}A (Narenpitak *et al.*, 2021), and kilometre-scale convection-permitting simulations have been shown to have some skill in reproducing this mechanism (Saffin *et al.*, 2023) and producing realistic variations in cloud organisation during EUREC^{4}A (Beucher *et al.*, 2022).

These results suggest that, given typical conditions in the trades during the dry season, the clouds should always tend towards more organised cloud patterns such as gravel or flowers. For example, the fish cloud pattern at the start of the EUREC^{4}A field campaign was associated with a trailing cold front and an extratropical dry intrusion, which is a relatively rare event, but has a strong impact on clouds and precipitation (Villiger *et al.*, 2022). Bony *et al.* (2020) showed that two environmental factors, namely inversion strength and low-level wind speed, are good indicators of which of the four cloud patterns would be present. Aemisegger *et al.* (2021) showed that the path that airmasses take to reach the region of interest had an important influence on the clouds. They described three regimes, namely extratropical dry intrusion, extratropical trade wind, and tropical, and showed that the location of Rossby wave breaking was important for the transport of air masses in the two extratropical regimes.

In this study we look at the synoptic features that occurred during EUREC^{4}A and how they link to cloud patterns. A knowledge-exchange workshop before the EUREC^{4}A field campaign brought together 16 forecasters from 12 countries, international researchers, and Caribbean lecturers to review the science and weather to be studied and forecasted in EUREC^{4}A. During the field campaign, forecasters conducted a virtual forecast "testbed" with daily weather discussions and forecast briefings to EUREC^{4}A scientists. The high-resolution model forecasts delivered for EUREC^{4}A by the UK Met Office and Météo-France were an opportunity for Caribbean forecasters to experience and evaluate the new generation of numerical weather prediction in an operational setting. Reciprocally, the insight of Caribbean forecasters and lecturers brought new insight to the EUREC^{4}A research teams, in interpreting the processes controlling

1477870x, 0, Downloaded from https://rmets.onlinelibrary.wiley.com/doi/10.1002/qj.70311 by Karlsruher Institut Fur Technologie, Wiley Online Library on [10/11/2026]. See the Terms and Conditions (https://onlinelibrary.wiley.com/terms-and-conditions) on Wiley Online Library for rules of use; OA articles are governed by the applicable Creative Commons License

the cloud fields every day. For example, some patterns identified as "fish" by the academic researchers were immediately identified to be pre-frontal cloud lines by the forecasters.

The presence of operational regional forecasters played an integral role in the overall outcome of the EUREC^{4}A programme. These forecasters were able to provide a comprehensive daily forecast of the synoptic driving factors, which in turn determined the expected weather. Given the expected weather, the EUREC^{4}A team was able to determine the type of cloud patterns to expect during their field operation. During the field operation, the forecasters were also able to provide some level of accuracy with respect to the time in which many of these cloud patterns are expected and the location where they are most likely to occur. A second workshop after the campaign consolidated knowledge gained from the forecast test-bed analysis, which formed the basis for this article.

This article aims to describe the synoptic features and large-scale circulation of the field campaign in a way that merges diagnostic analysis from model fields with insight into synoptic dynamics and structures. The article will outline in detail the synoptic conditions during the EUREC^{4}A field campaign and how they relate to cloud patterns. It is structured as follows: in Section 2 we describe the known synoptic and large-scale drivers of dry-season weather and climate in the Caribbean region; in Section 3 we describe the datasets used in this article; in Section 4.1 we subjectively split the EUREC^{4}A field campaign into four periods and describe the important synoptic features for each period; in Section 4.3 we summarise the synoptic features identified in Section 4.1 and compare and contrast across the different time periods; and in Section 5 we provide the conclusions.

2 | LARGE-SCALE AND SYNOPTIC DRIVERS OF DRY-SEASON WEATHER AND CLIMATOLOGY

The weather of the Caribbean region is controlled by synoptic structures, some of which are globally familiar and some of which are specific to this climatic region. In this section we describe the relevant features that are included on a typical synoptic chart used by forecasters in the Caribbean. The analysis in this article was aided by synoptic charts produced by Météo-France Antilles-Guyane. These synoptic charts are produced following Santurette and Joly (2002) with modifications from Lafore *et al.* (2017) for tropical charts. Figure 1 shows an example synoptic chart.

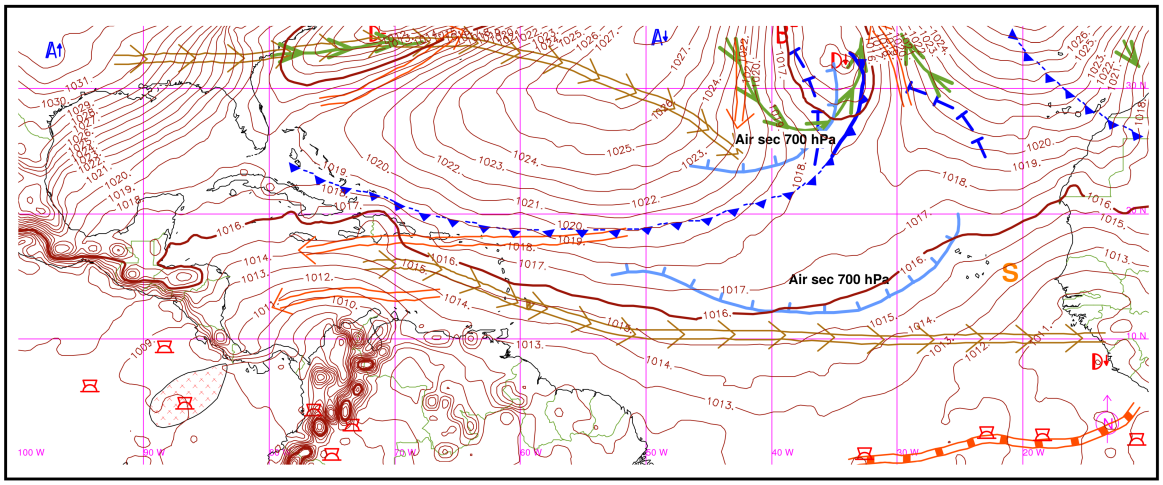
The subtropical jet is a nearly continuous fast-flowing airstream in the upper troposphere and can be seen on the synoptic chart stretching from the Caribbean to West Africa. The incursion of the subtropical jet is strongest during the dry season. The variability of the subtropical jet and associated troughs can occasionally provide enhancement for cloud development and instigate moderate to heavy showers depending on its location in relation to instability at the surface (Pfahler *et al.*, 2025). Although the upper tropospheric troughs shown in the example chart are far from the Caribbean, they do often influence the region.

The dry season is characterised by the dominance of the subtropical high across the Atlantic associated with descending air in the lower troposphere. In the example synoptic chart, the high pressure is located in the central North Atlantic. Typically in winter, the centre of this subtropical high is generally in the region of the Azores, whereby it is called the Azores High. Despite the centre of the high pressure being more eastward in the winter, a tighter pressure gradient in the tropical Atlantic results in the increase in trade wind speeds across the region. The Azores High often contributes to strong northeasterly winds generally between 10°N and 15°N—across Barbados and the southeastern Caribbean islands. In addition, its influence can cause shallow cloud patches depending on proximity and strength. The movement of the trade winds over the tropical Atlantic causes ocean upwelling in the eastern Atlantic (near the high centre), cooling the upper ocean and creating a gradient in sea-surface temperatures, which in turn maintains the pressure gradient at the surface (higher to the east, lower to the west). Subsidence warming in the region of high pressure and the cooler water due to upwelling then creates a temperature inversion over the eastern tropical Atlantic called the trade wind inversion. This inversion caps the cumulus layer and weakens westward and equatorward (away from the high-pressure centre); thus, clouds tend to be shallower in the eastern Atlantic and deeper away from the centre.

Extratropical low-pressure systems and their associated fronts can also influence the weather in the Caribbean, although less frequently and more transient than the influence of the high pressure. The example synoptic chart shows a low-pressure system in the Atlantic with a long trailing cold front extending over the Caribbean.

The intertropical convergence zone (ITCZ) is identified in the southeast corner of the synoptic chart with associated convection. The ITCZ is a feature that is caused by northeast and southeast trade winds converging and is characterized by a band, or bands, of well-developed clouds along or near the Equator. The ITCZ is a semi-permanent feature that oscillates according to the seasons. By January (winter), the ITCZ migrates southward as a result of the Northern Hemisphere's winter while cold air advances southeastward across the

1477870x, 0, Downloaded from https://rmets.onlinelibrary.wiley.com/doi/10.1002/qj.70311 by Karlsruher Institut Fur Technologie, Wiley Online Library on [10/11/2026]. See the Terms and Conditions (https://onlinelibrary.wiley.com/terms-and-conditions) on Wiley Online Library for rules of use; OA articles are governed by the applicable Creative Commons License



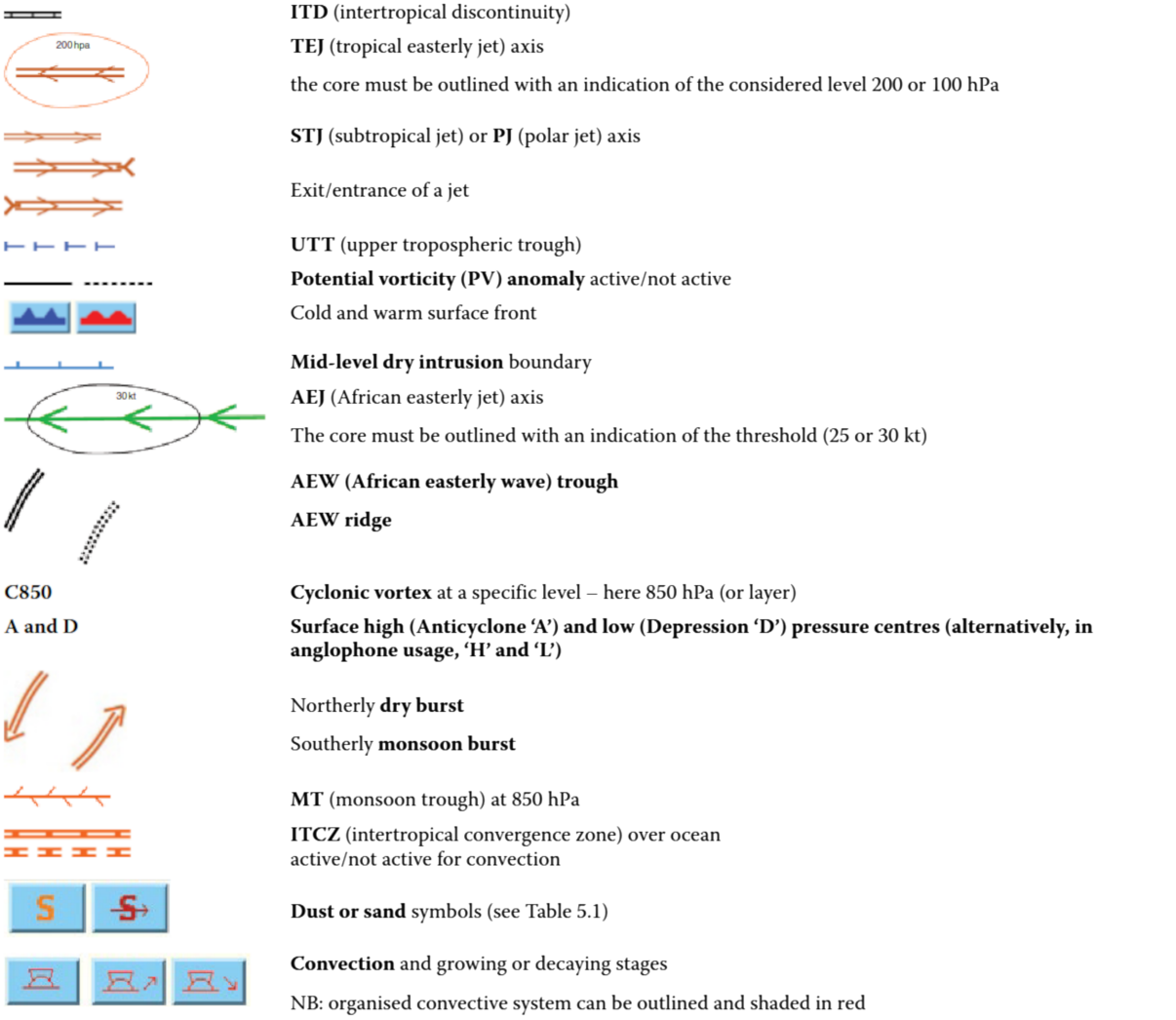


FIGURE 1 Synoptic chart produced by Météo-France Antilles-Guyane for January 20, 2020, with the key copied from in Lafore *et al.* (2017, table 11.1). The green arrows are shown as the African easterly jet axis in the key, but they are also used for jet regions in the extratropics. There is no African easterly jet or associated ridges or troughs in the chart shown, but they are kept in the legend.

1477870x, 0, Downloaded from https://rmets.onlinelibrary.wiley.com/doi/10.1002/qj.70311 by Karlsruher Institut Fur Technologie, Wiley Online Library on [10/11/2026]. See the Terms and Conditions (https://onlinelibrary.wiley.com/terms-and-conditions) on Wiley Online Library for rules of use; OA articles are governed by the applicable Creative Commons License

Caribbean region, resulting in reduced temperatures and occasional shear lines. By July this motion reverses as the ITCZ migrates slightly northward as a transition to the Southern Hemisphere winter begins. The midlevels are moist within the ITCZ but dry to the north and south. Dry air intrusions can occur here and tend to be associated with significant weather at their leading edge.

The trade winds can lead to the transport of dust and aerosol from the Sahara and West Africa across the Atlantic to the Caribbean. A dust airmass is seen on the synoptic chart off the west coast of Africa in Figure 1.

3 | DATA

In the following sections we use a mix of observational and reanalysis data to show the local conditions and synoptic features during the EUREC^{4}A field campaign. Though more data were used during the workshop and much more detailed observations are available for the field campaign (Stevens *et al.*, 2021), we have limited the data shown here to a small subset of data with continuous coverage of the field campaign.

To show the synoptic features, we have used potential vorticity (PV), specific humidity, winds, and mean-sea-level pressure (MSLP) from the fifth-generation European Centre for Medium-Range Weather Forecasts Reanalysis (ERA5; Hersbach *et al.*, 2020). We have also used the ERA5 data to calculate mass flux associated with the Hadley circulation (see Section 4.2). As ERA5 does not include aerosol, we have used the aerosol optical depth from Modern-Era Retrospective Analysis for Research and Applications version 2 (MERRA-2; Gelaro *et al.*, 2017). We have reproduced GEOColor composite visible images—following Miller *et al.* (2020)—over the region of interest using data from the GOES-16 satellite (Knapp, 2017). We also used the compilation of observed cloud patterns over Barbados from visible satellite imagery from the C^{3}ONTEXT dataset (Schulz *et al.*, 2021).

To show the local conditions in Barbados we use observations from the Barbados Cloud Observatory located at Ragged Point in Barbados (Stevens *et al.*, 2016). We have included rain and wind speed and direction. We have also included cloud fraction derived from observations from the Ka-band cloud radar following the example from EUREC^{4}A Community (2026). We have also included measurements of aerosol properties that were made at Ragged Point using a GRIMM optical particle counter over the size range $0.3 < d_p < 32\,\mu m$. To examine variability in the vertical structure of the atmosphere through the study period, we have utilised the radiosonde soundings released from Grantley Adams Airport in Barbados, with the data accessed via the University of Wyoming upper air database (Wyoming, 2015).

The code to reproduce the figures in this article has been archived in a zenodo repository alongside the synoptic charts for the field campaign period (Saffin, 2026).

4 | RESULTS

This section combines a quantitative analysis of synoptic patterns with synoptic analysis to document the evolution of weather types during the campaign, and their influence on the prevailing cloud environments.

4.1 | Analysis of four periods during EUREC^{4}A

Figure 2 shows the cloud patterns and aerosol particle concentration (see Section 3) observed at Barbados during the EUREC^{4}A field campaign. The cloud pattern time series highlights that through the January 20–24 period there is a predominance of the fish cloud pattern. There is then a period (January 25–28) where the pressure gradient slackens and winds are light, with no predominant low-level cloud type through this time. Following this period we see days that develop the flowers cloud pattern interspersed with days with varying amounts of the gravel and sugar cloud patterns and least frequently the fish cloud pattern. Later on (from February 8), we see a mixture of all cloud patterns identified, with much less unclassified cloud patterns. This is associated with increased rain amounts and deeper clouds.

There are two periods of increased aerosol during EUREC^{4}A (Figure 4.1c). Although it is difficult to detect the origin of aerosols from the data used in this study, to say whether it is dust or other aerosol, Gutleben *et al.* (2022) have analysed the dust transport during EUREC^{4}A and have shown that mineral dust aerosols were transported at lower altitudes below 3.5 km. They calculated backward trajectories, which confirmed that mineral dust was transported across the North Atlantic. Gutleben *et al.* (2022) found from lidar observations that the aerosol detected near Barbados was a mixture of dust particles and other aerosol species; that is, biomass-burning aerosol from fires in West Africa and marine aerosol. This study also showed that the dust-laden air had enhanced water vapour concentrations. Cuevas-Agulló *et al.* (2024) have shown that, in February and March 2020–2022, several intense dust intrusions occurred over northern Africa.

Based on the time series and experience from the field campaign, we have divided the EUREC^{4}A field campaign into four periods of interest:

1477870x, 0, Downloaded from https://rmets.onlinelibrary.wiley.com/doi/10.1002/qj.70311 by Karlsruher Institut Fur Technologie, Wiley Online Library on [10/11/2026]. See the Terms and Conditions (https://onlinelibrary.wiley.com/terms-and-conditions) on Wiley Online Library for rules of use; OA articles are governed by the applicable Creative Commons License

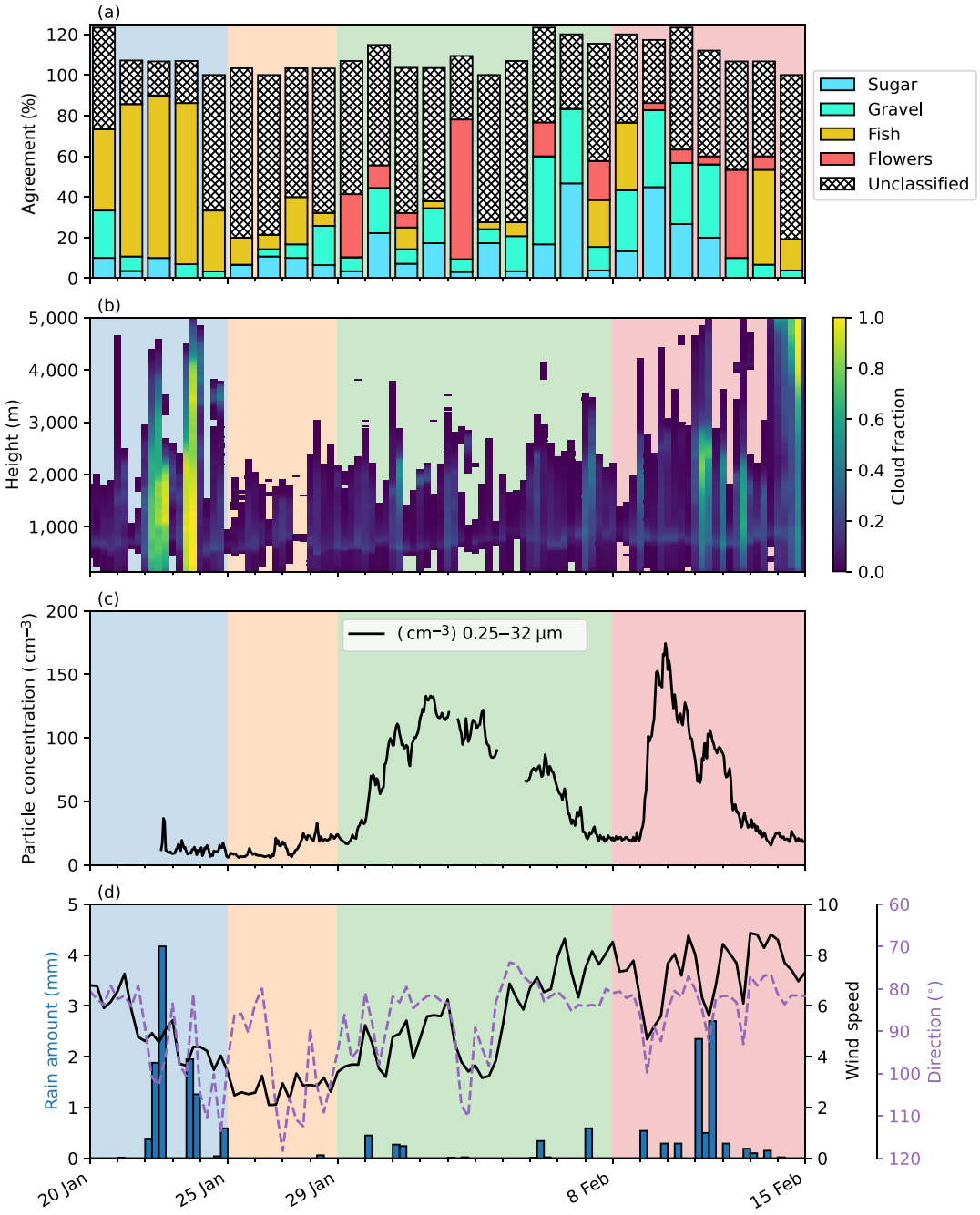


FIGURE 2 Time series of observations from Barbados during EUREC⁴A. (a) Daily average cloud pattern at the Barbados Cloud Observatory (BCO) reproduced from Schulz (2022, fig. 5a). (b) Six-hourly averaged cloud fraction from the cloud radar at BCO. (c) Particle concentration in number per cubic centimetre of aerosol particles in the size range 0.25–32 µm measured by the GRIMM optical particle counter. (d) Six-hourly accumulated rain, and six-hourly averaged wind speed (ms^{-1}) and direction observed at BCO. The wind direction is degrees from north (i.e., 90° is an easterly wind). The background colours show the four subjectively identified time periods.

1. **January 20–24**, fish clouds;
2. **January 25–28**, quiet period for cloud development;
3. **January 29–February 7**, cloud development and first dust event;
4. **February 8–14**, deeper cloud development and second dust event.

Though the EUREC⁴A observational campaign did continue beyond February 14, we conclude our study period here. The increase in midlevel moisture and clouds, associated with flow from South America/Brazil (Villiger *et al.*, 2022), obscured the shallow cumulus clouds, making it impossible to determine low-level cloud patterns in

1477870x, 0, Downloaded from https://rmets.onlinelibrary.wiley.com/doi/10.1002/qj.70311 by Karlsruher Institut Fur Technologie, Wiley Online Library on [10/11/2026]. See the Terms and Conditions (https://onlinelibrary.wiley.com/terms-and-conditions) on Wiley Online Library for rules of use; OA articles are governed by the applicable Creative Commons License

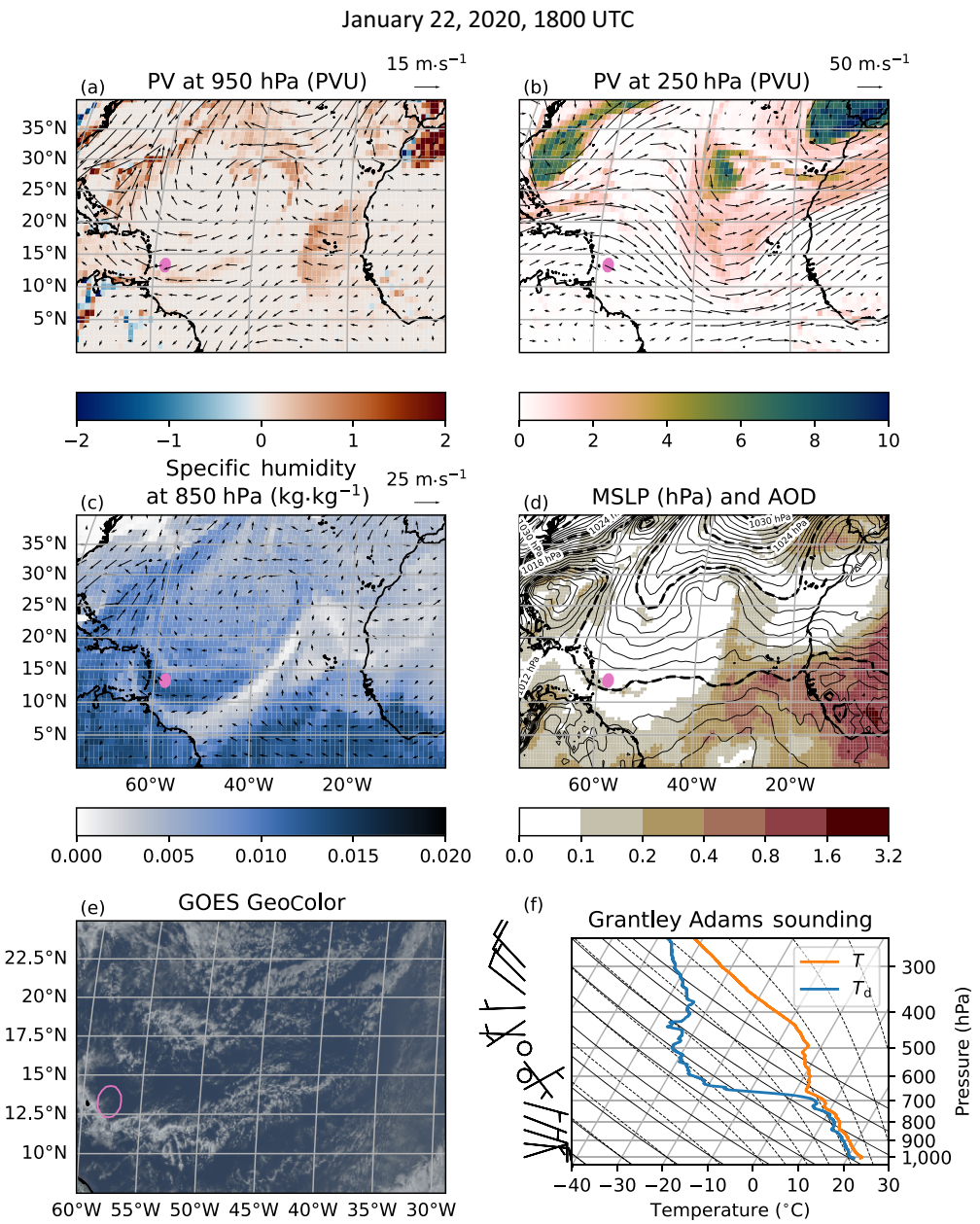


FIGURE 3 Reanalysis and observational data for January 22 at 1800 UTC. (a) Fifth-generation European Centre for Medium-Range Weather Forecasts Reanalysis (ERA5) potentil vorticity (PV) and wind vectors at 950 hPa. (b) ERA5 PV and wind vectors at 250 hPa. (c) ERA5 specific humidity and wind vectors at 850 hPa. (d) ERA5 mean-sea-level pressure (MSLP; contours every 1 hPa and dashed every 6 hPa) and Modern-Era Retrospective Analysis for Research and Applications version 2 aerosol optical depth (AOD; colours, logarithmic scale). (e) GOES GeoColor composite of visible channels following Miller *et al.* (2020). (f) Skew-*T* log-*P* chart of the sounding from Grantley Adams Airport at 1200 UTC. The wind barbs are in increments of 10 m · s^{-1} (5 m · s^{-1} for half barbs). The pink circle to the west of Barbados in panels (a)–(e) shows main measurement area during the EUREC^{4}A field campaign.

visible satellite imagery. This can be seen in the increase in cloud fraction and the higher proportion of unclassified cloud patterns at the end of Figure 2.

In the following section we show various meteorological variables to give an overview of the synoptic situation and cloud patterns associated with each period. Figures 3–6 show snapshots of various fields from reanalysis data and observations. The panels of each figure show the following:

1. *Low-level (950 hPa) wind and PV*. The low-level winds are useful for showing the strength and direction of the trade winds. PV is useful for showing fronts and shear lines (particularly important for the fish clouds in the first period of interest).
2. *Upper-level (250 hPa) wind and PV*. The upper-level winds help to show the influence of the subtropical jet. PV shows a more coherent picture of the subtropical jet and the associated sharp contrast between tropospheric low-PV air and stratospheric high-PV air. The PV then clearly shows the Rossby wave activity and particularly the influence of ridges and troughs as well as PV streamers, associated with Rossby wave breaking in the midlatitudes, extending towards the region of interest.
3. *Low-to-mid-level (850 hPa) wind and specific humidity*. The winds give an idea of the wind shear when compared with panel (a), and the moisture gives an idea of the potential for convection.

1477870x, 0, Downloaded from https://rmets.onlinelibrary.wiley.com/doi/10.1002/qj.70311 by Karlsruher Institut Fur Technologie, Wiley Online Library on [10/11/2026]. See the Terms and Conditions (https://onlinelibrary.wiley.com/terms-and-conditions) on Wiley Online Library for rules of use; OA articles are governed by the applicable Creative Commons License

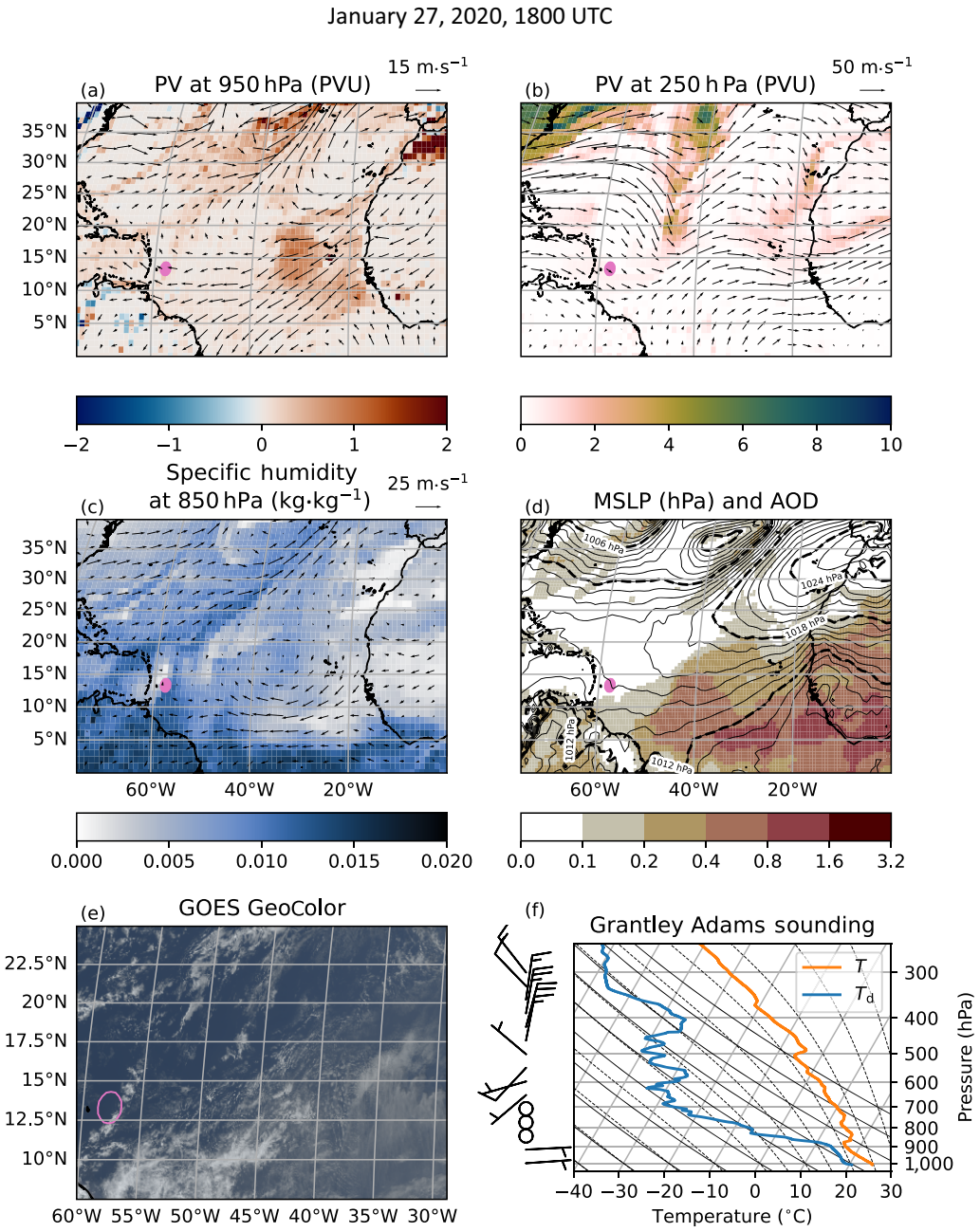


FIGURE 4 Same as Figure 3 but for January 27.

4. *MSLP and aerosol optical depth*. The MSLP is useful for understanding the low-level winds' strength and direction and shows how they are largely influenced by midlatitude high- and low-pressure systems. The aerosol optical depth is shown to trace back the origins of the dust events in Barbados and their transport from West Africa.
5. *Colour composite satellite images using visible channels from the GOES satellite*. The purpose of these figures is to give an overview of the clouds and cloud patterns. For an overview of satellite imagery and cloud patterns for the full EUREC^{4}A period see Schulz (2022, app. A).
6. *Radiosonde soundings from Grantley Adams Airport in Barbados*. The soundings are included to determine the convective instability, low-level moisture, the depth of (potential) cloud layers, inversion strength, and wind shear.

We only show one figure for each variable for each period. We have placed the figures for each day and the code to produce them in a zenodo repository (Saffin, 2026).

1477870x, 0, Downloaded from https://rmets.onlinelibrary.wiley.com/doi/10.1002/qj.70311 by Karlsruher Institut Fur Technologie, Wiley Online Library on [10/11/2026]. See the Terms and Conditions (https://onlinelibrary.wiley.com/terms-and-conditions) on Wiley Online Library for rules of use; OA articles are governed by the applicable Creative Commons License

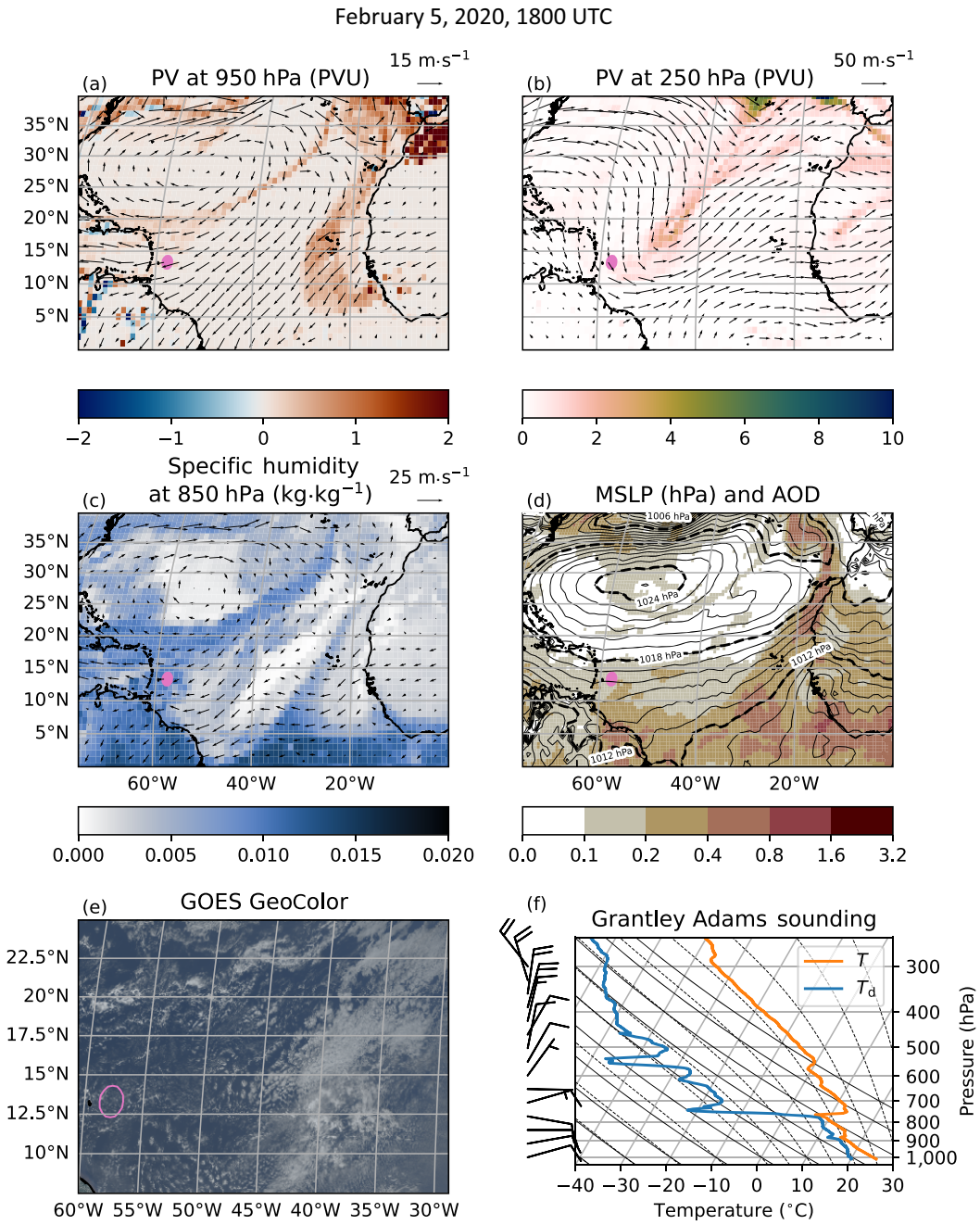


FIGURE 5 Same as Figure 3 but for February 5.

4.1.1 | January 20–24: Shear line and fish clouds

During the first part of the EUREC^{4}A field campaign the conditions across the study region were influenced by a midlatitude depression over the central Atlantic. Figure 3 shows a southwest–northeast-oriented shear line extending from 20°N, 35°W towards the Caribbean: it can also be observed in both the 950 hPa PV field and enhanced moisture in the 850 hPa specific humidity field. The shear line moves southwards across the Lesser Antilles through this period. The pattern with the depression centred in the mid-Atlantic creates a relatively sharp pressure gradient and drives near-surface easterly winds across the tropical Atlantic. The radiosonde sounding from 1200 UTC on January 22 (Figure 3f) highlights the easterly flow in the boundary layer, and there is significant wind shear with westerly winds associated with the subtropical jet aloft (350 to 150 hPa). Further, the sounding highlights a transition from moist air between 1,000 and 700 hPa (surface to approximately 3 km altitude) and drier air aloft (700–400 hPa).

1477870x, 0, Downloaded from https://rmets.onlinelibrary.wiley.com/doi/10.1002/qj.70311 by Karlsruher Institut Fur Technologie, Wiley Online Library on [10/11/2026]. See the Terms and Conditions (https://onlinelibrary.wiley.com/terms-and-conditions) on Wiley Online Library for rules of use; OA articles are governed by the applicable Creative Commons License

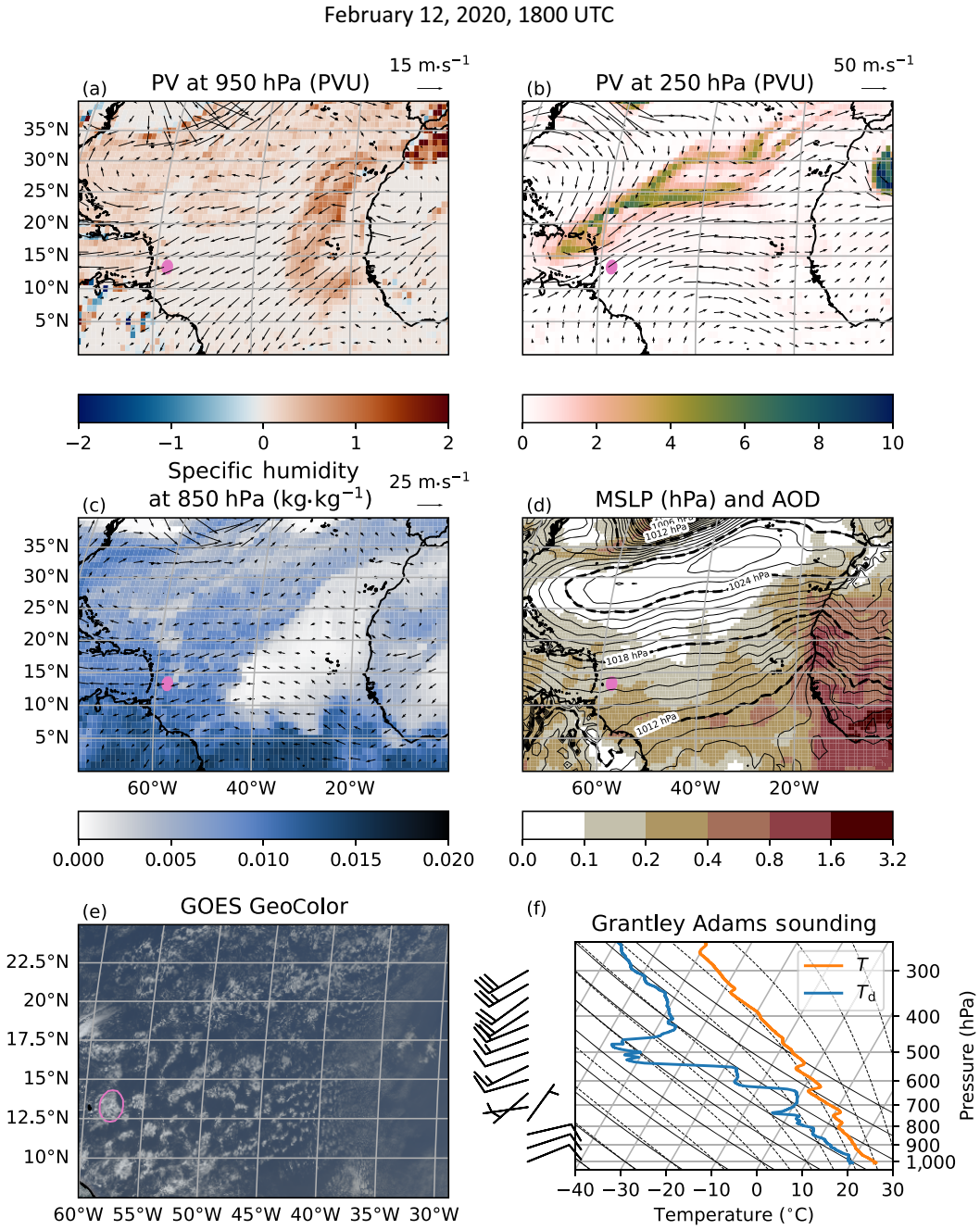


FIGURE 6 Same as Figure 3 but for February 12.

From January 20 to January 24 the shear line and associated low-level moisture produced organised and significant cloud cover over Barbados (Figure 3e), with some light rain and showers reported. From January 25 onwards the influence of the shear line decreased as it moved southwards, with reduced cloud amounts across the study region. Analysis of additional radiosonde profiles from January 24 and January 25 highlight a drying of the 1,000 hPa to 700 hPa layer—marking the onset of a quieter period with reduced cloud (see Figure 2a).

4.1.2 | January 25–28: Quiet period

The start of this period is marked by a transition from a relatively strong pressure gradient and easterly winds across the study region to quieter conditions, light winds, and a ridge of high pressure building from January 27 onwards. There is a weak Azores High that is shifted northeast and very zonal trade winds, compared with the following period where a new, stronger, high-pressure system dominated the subtropical North Atlantic and is associated with more northwesterly trade winds. On January 25 and 26 a

1477870x, 0, Downloaded from https://rmets.onlinelibrary.wiley.com/doi/10.1002/qj.70311 by Karlsruher Institut Fur Technologie, Wiley Online Library on [10/11/2026]. See the Terms and Conditions (https://onlinelibrary.wiley.com/terms-and-conditions) on Wiley Online Library for rules of use; OA articles are governed by the applicable Creative Commons License

weak and decaying shear line brings organised cirrus cloud across the study area, as shown by the satellite image in Figure 4e. Through the rest of the period the radiosonde profiles from Barbados show the dry air extending to lower levels (e.g., down to 850 hPa in Figure 3f), which inhibits convective cloud development in the study region (see Figure 2).

4.1.3 | January 29–February 7: First dust event and periods of developing clouds

During the third period there was a mixture of conditions, with days where cloud organisation developed quite readily with research flights through flowers cloud patterns on February 2, 5, and 7 and other days that were relatively quiet. The flowers and gravel cloud patterns do not dominate as much as the fish cloud pattern in the first period (Figure 2a). The flowers cloud pattern develops upstream from regions that might initially be described as sugar (e.g., Narenpitak *et al.*, 2021), so the weaker dominance of these cloud patterns is both space and time dependent. This can be seen in Figure 5e, where the flowers cloud pattern in the HALO circle has not developed yet, but the region just upstream (55°W, 13°N) is starting to develop.

The upper-level PV (Figure 5b) shows increased wave activity in the subtropical jet and associated PV streamers that are sometimes over the region of interest through this period. We found that the development of the more organised cloud patterns (flowers/gravel) during this period were always associated with a trough or PV streamer. The influence and strength of the subtropical high in the central Atlantic continues to dominate, with low- and midlevel easterly flow across the tropical Atlantic towards the region of interest.

On the days where research flights were conducted, the radiosonde profiles are characterised by a moist layer extending up to the 800 hPa or higher (see Figure 5f for an example). There is a sharp transition between moist air in the boundary layer and dry air in the free troposphere, with a strong capping temperature inversion at 750 hPa. Note that the inversion height varies between 800 and 700 hPa through the period, with a smooth "capping" inversion in places and spatial variation in the details seen from the dropsondes around the HALO circle (George *et al.*, 2021). Previous work by Bony *et al.* (2020) has shown that a stronger inversion is linked to an increased likelihood of developing the flowers cloud pattern that was observed sporadically through this period. There are differences in the radiosonde profiles through this period: February 2, 4, 5, and 7 are characterised by capping inversions between 850 and 700 hPa of varying sharpness; on February 3 and 6 the boundary layer is more weakly capped and there is less near-surface moisture (not shown).

Near-surface winds are also stronger through this period, increasing from 4 to 8 $m \cdot s^{-1}$ through the period (Figure 2d). The strength of near-surface easterly winds also appears to be linked to the tendency for more frequent identification of flowers and gravel cloud patterns through this period (Figure 2a), consistent with Bony *et al.* (2020), although the day most dominated by the flowers cloud pattern (February 2) does show a sharp drop in wind speed and change in wind direction.

Through this period there is a gradual increase in aerosol followed by a decrease from February 2 (see Figure 2c) as mineral dust was advected westwards across the Atlantic on the southern flank of the anticyclone that extends towards the Lesser Antilles (Chazette *et al.*, 2022). The initial transport of this dust plume away from the west coast of Africa occurs in the first period (see Figure 3d). In the visible satellite imagery there are often clouds resembling those in the flowers cloud pattern on the leading edge of the mineral dust plume (e.g., Figure 5d,e, around 45°W, 15°N). These flowers-type clouds on dust boundaries were noted on multiple days, particularly at the start of the period when the dust plume is initially moving towards Barbados. Since the flowers-type clouds form along a line they could be present in satellite images without being the dominant cloud pattern.

On various days during this period we see small amounts of the fish cloud pattern identified (Figure 2a). In contrast to the first period, where the fish pattern dominates the region and is clearly associated with a front/shear line, the cloud patterns that were identified as fish appear to be smaller scale and not associated with any clear synoptic feature.

4.1.4 | February 8–14: Deeper cloud development and second dust event

The subtropical high pressure in the central Atlantic continues to dominate the synoptic pattern through this period. The anticyclone elongates in an west–east orientation, somewhat enhancing the pressure gradient across the Caribbean and strengthening near-surface easterly winds. At upper levels there is a series of PV streamers through this period that extend from the Caribbean northeastwards into the subtropical Atlantic. These features typically enhance the potential for deeper convection, though they mainly stay to the north of the EUREC^{4}A study region until February 14. The upper-level southwesterly winds associated with one of these streamers (February 12–15) brings the onset of more moisture through the midtroposphere and arrival of midlevel clouds.

1477870x, 0, Downloaded from https://rmets.onlinelibrary.wiley.com/doi/10.1002/qj.70311 by Karlsruher Institut Fur Technologie, Wiley Online Library on [10/11/2026]. See the Terms and Conditions (https://onlinelibrary.wiley.com/terms-and-conditions) on Wiley Online Library for rules of use; OA articles are governed by the applicable Creative Commons License

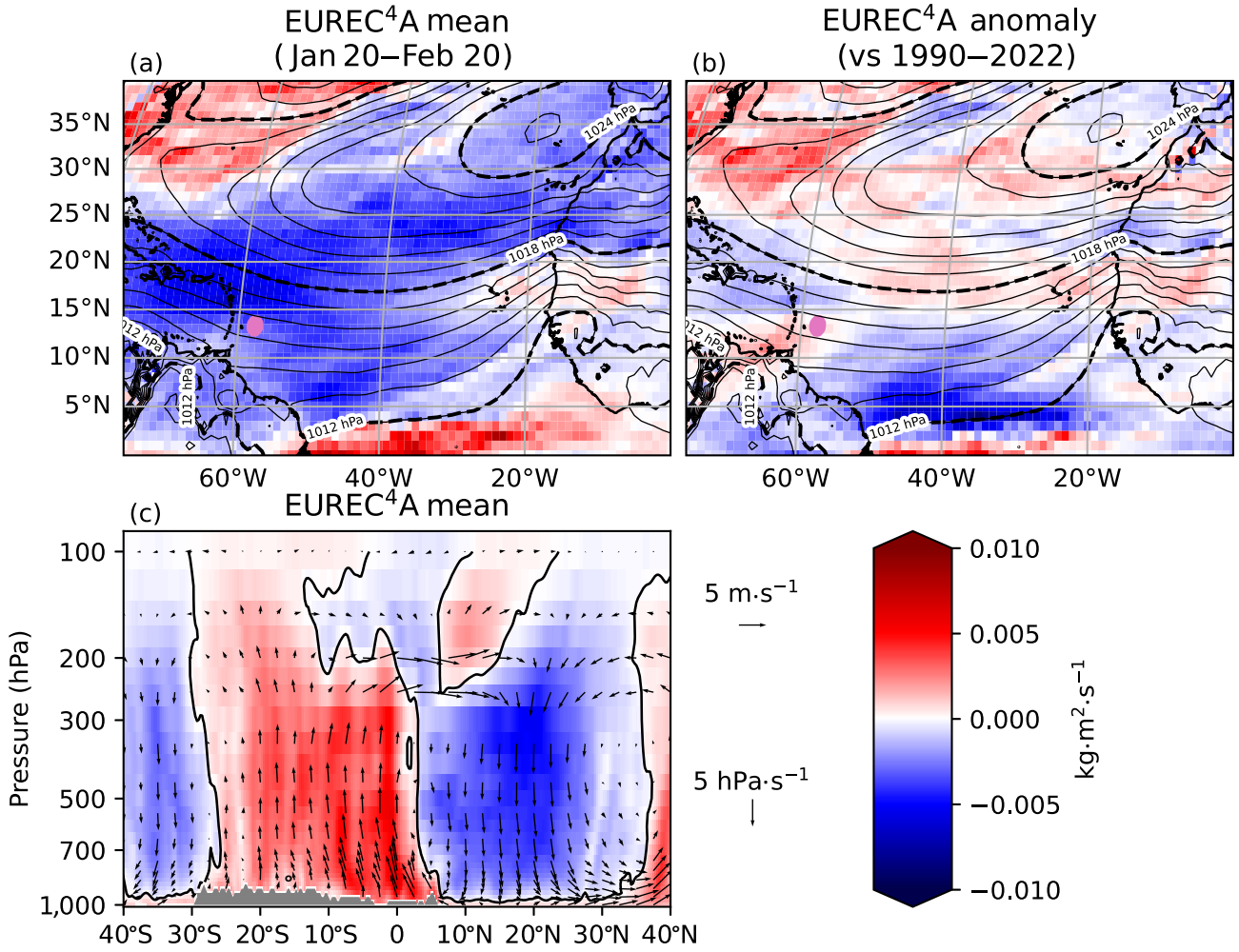


FIGURE 7 (a) The mean meridional mass flux (shaded, $kg \cdot m^{-2} \cdot s^{-1}$) at 500 hPa and the mean mean-sea-level pressure (MSLP; contours, hPa) over the EUREC⁴A field campaign period (January 20–February 20). (b) The anomaly of the meridional mass flux from the 1990–2022 mean over the same dates (shaded, $kg \cdot m^{-2} \cdot s^{-1}$) at 500 hPa and the mean MSLP (contours, hPa). (c) The mean meridional mass flux (shaded, $kg \cdot m^{-2} \cdot s^{-1}$) and the wind in the plane of the cross-section (arrows, $m \cdot s^{-1}$) over the EUREC⁴A field campaign period averaged between 60°W to 40°W. These plots are based on fifth-generation European Centre for Medium-Range Weather Forecasts Reanalysis data.

In the region of interest, there is a slow transition through the early part of this period with a gradual deepening of the boundary layer and increased near-surface moisture. By February 12 this near-surface moist layer extends up to 600 hPa (see Figure 6f). This allows the depth of clouds to increase through the period, with convective clouds being deep enough to generate light rain showers in the vicinity of Barbados. The profile in Figure 6f is characteristic of the period, with a sharp transition to dry air at the top of a relatively deep moist layer. Throughout the period there is a strong westerly jet in the upper troposphere (approximately 250 hPa) that is associated with enhanced vertical wind shear.

The cloud patterns during this period are similar to the previous period, with the flowers and gravel patterns frequently developing from sugar. In the transition from the previous period (February 7–8) there are some fish cloud patterns identified (Figure 2a). This fish cloud pattern is larger scale than those embedded within other cloud patterns in the previous period, but also not as dominant or associated with a clear front as in the first period.

4.2 | Local Hadley circulation

The local Hadley circulation during the EUREC⁴A field campaign period was analysed using the ψ-vector method outlined in Schwendike *et al.* (2014). The meridional mass flux averaged from January 20 to February 20, 2020, is shown in Figure 7a. In alignment with the areas of relatively high MSLP in the subtropical and tropical Atlantic, downward mass flux can be found. The strongest downward mass flux occurs over the Caribbean and is part of

14778780x, 0, Downloaded from https://rmets.onlinelibrary.wiley.com/doi/10.1002/qj.70311 by Karlsruher Institut Fur Technologie, Wiley Online Library on [10/11/2026]. See the Terms and Conditions (https://onlinelibrary.wiley.com/terms-and-conditions) on Wiley Online Library for rules of use; OA articles are governed by the applicable Creative Commons License

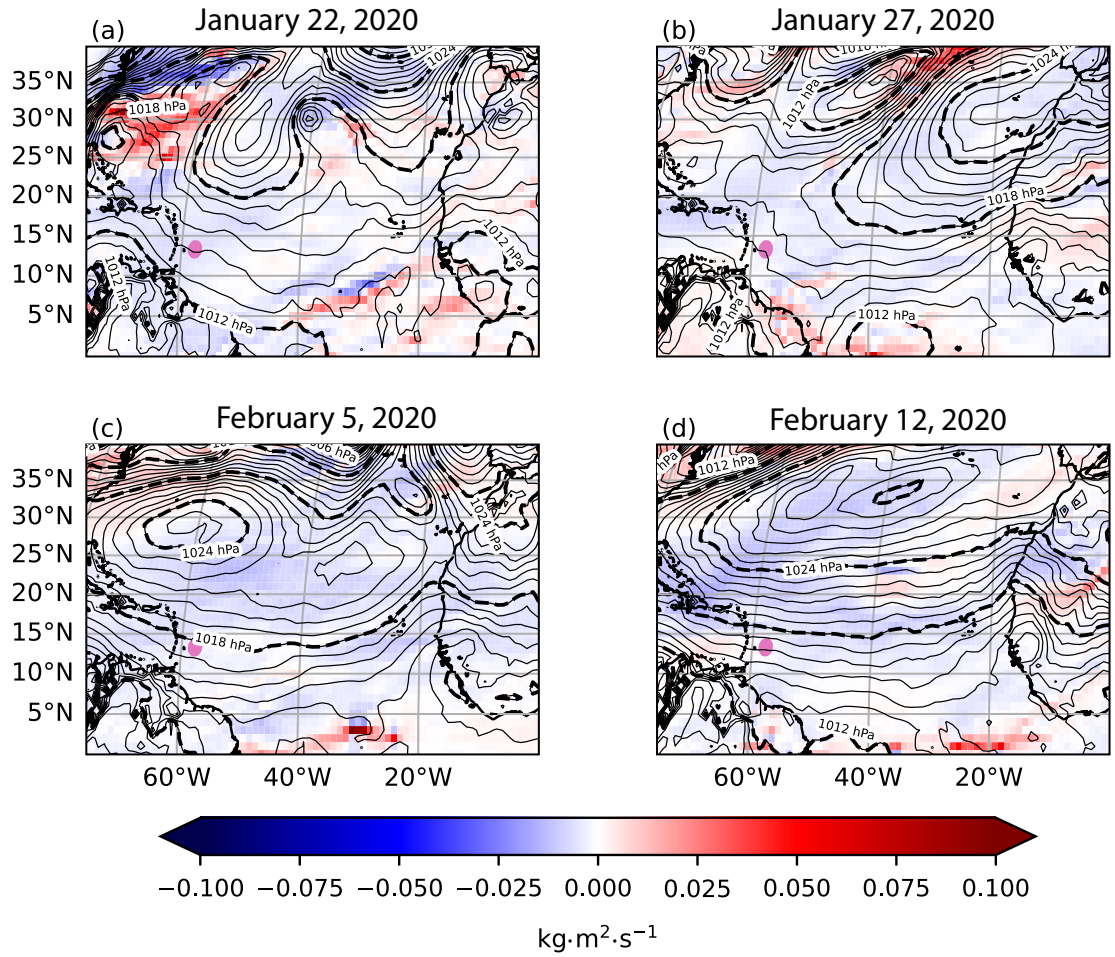


FIGURE 8 The daily mean meridional mass flux at 500 hPa (shaded, kg · m^{-2} · s^{-1}) and mean mean-sea-level pressure (contours, hPa) at four times during the EUREC^{4}A field campaign period.

the descending branch of the local Hadley circulation. The ascending branch of the local Hadley circulation can be seen in the equatorial Atlantic and in the eastern Pacific. In the midlatitudes the meridional mass flux should be interpreted as the meridional component of the three-dimensional circulation and will not represent the local Hadley circulation.

The anomalies in the meridional mass flux during the field campaign and the mean between 1990 and 2022 are shown in Figure 7b. This plot shows that there is anomalously negative mass flux (i.e., stronger descent) over the Caribbean. Barbados and the field campaign region are located in a region of enhanced mass flux. The anticyclone over the Atlantic is weaker than in the mean, and the ascending branch of the local Hadley circulation is shifted further south than in the mean.

The mean regional Hadley circulation averaged between 60°W to 40°W is shown in Figure 7c. This plot extends to the Southern Hemisphere to show both branches of the local Hadley circulation during the EUREC^{4}A period. As expected, the strongest descent occurs in the winter hemisphere and the strongest ascent is located in the summer hemisphere.

Figure 8 shows that there is day-to-day variability in the meridional vertical mass flux and that the mass flux distribution on a given day and time could look quite different from the mean over the EUREC^{4}A period (Figure 7). The local Hadley circulation on January 22 and 27 and on February 5 and 12 at 1800 UTC is shown in Figure 8. The most evident features in upward and downward mass flux are those associated with weather systems in the midlatitudes. The mass flux in the EUREC^{4}A region is positive, but the values are low, on January 22 and 27 and February 5, and both positive and negative on February 12. On this day the downward mass flux over the Atlantic is more widespread in comparison with the other days.

Vertical cross-sections of the local Hadley circulation averaged between 60°W to 40°W are shown in Figure 9. Comparing Figures 9 and 7c shows that at individual times the large-scale circulation is characterised by smaller-scale features. The ascending and descending branches of the local Hadley circulation are still evident, but, in particular,

1477870x, 0, Downloaded from https://rmets.onlinelibrary.wiley.com/doi/10.1002/qj.70311 by Karlsruher Institut Fur Technologie, Wiley Online Library on [10/11/2026]. See the Terms and Conditions (https://onlinelibrary.wiley.com/terms-and-conditions) on Wiley Online Library for rules of use; OA articles are governed by the applicable Creative Commons License

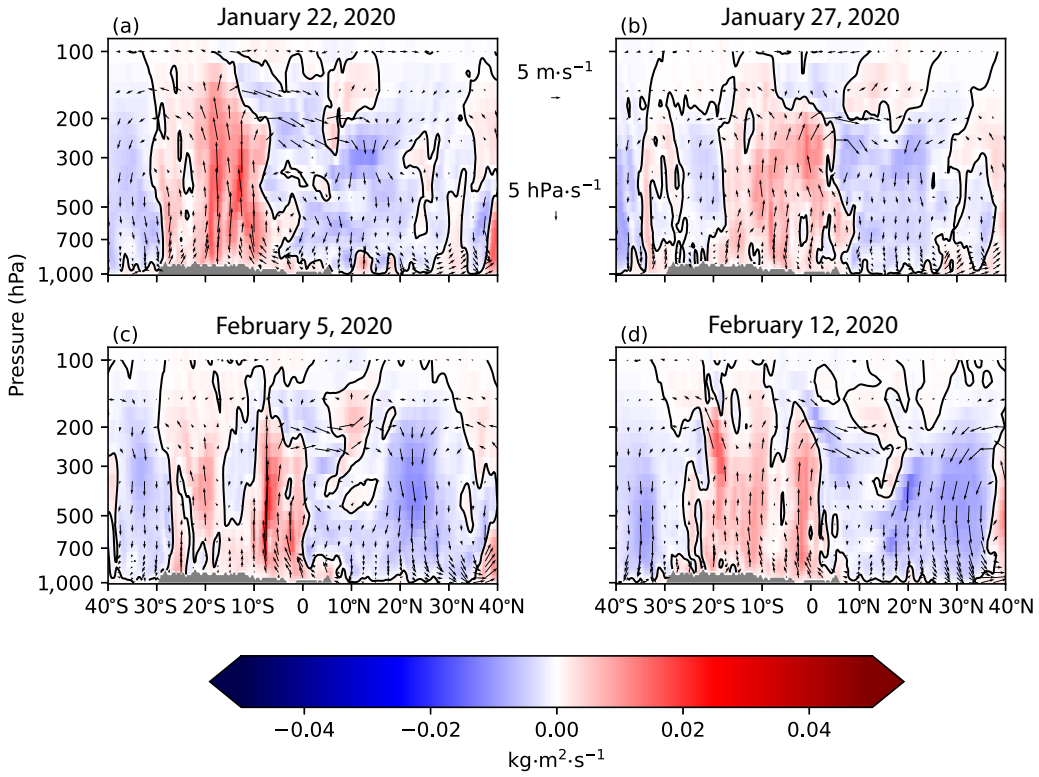


FIGURE 9 Vertical cross-sections of the daily mean meridional mass flux (shaded, $kg \cdot m^{-2} \cdot s^{-1}$) and the the wind in the plane of the cross-section (arrows, $m \cdot s^{-1}$) averaged over 60°W to 40°W at four times during the EUREC^{4}A field campaign period.

the region of ascent is interspersed by regions of descent. Over the tropical Atlantic, the strength of the downward mass flux varies. The downwards mass flux is stronger in Figure 9b at about 10–20°N, and regions of ascent occur at the other times.

4.3 | Summary of synoptic features

The main synoptic features and cloud types in the Barbados area during each of the four periods of the EUREC^{4}A field campaign are summarised in Figure 10.

1. Period 1 was characterised by the elongated shear line stretching across the North Atlantic and was linked to an elongated upper-level PV trough. "Fish" clouds developed in the Tropics along the shear line.
2. In the transition from period 1 to period 2 the impact of the midlatitude Rossby waves reduced and the region around Barbados was characterised by a lack of synoptic-scale influence. This period had the most "unclassified" cloud patterns, which was found to generally be clear sky or a mix of sugar-like cloud patterns and other clouds. There were also occasional small-scale fish cloud patterns. Throughout periods 1 and 2 the dry and dust-enriched air coming off the west coast of Africa was moving westwards across the Atlantic.
3. In period 3 this dry and dusty air has reached the field campaign region. During period 3 a shear line as an extension of a midlatitude cold front reached all the way to the Bermudas but did not move further south. The cloud patterns during this period were characterised by sugar with intermittent development of the flowers or gravel cloud patterns, and sometimes all three cloud patterns identified in the same satellite image. The fish cloud pattern was also occasionally identified, but smaller scale and less dominant than in the first period. The predominant cloud patterns evolve through time, and it could be argued that the airmass in which the flowers cloud pattern develops would have been earlier classified as sugar.
4. Two prominent high-pressure systems in the North Atlantic combined to one big and elongated high-pressure system that extended over most of the North Atlantic in the transition from period 3 to period 4. The dusty and dry air is also retreating. Similar to the previous period, the cloud patterns during this period were characterised by sugar with intermittent development of the the flowers or gravel cloud patterns. Compared with the previous period, the clouds were deeper and brought more rain to Barbados.

1477870x, 0, Downloaded from https://rmets.onlinelibrary.wiley.com/doi/10.1002/qj.70311 by Karlsruher Institut Fur Technologie, Wiley Online Library on [10/11/2026]. See the Terms and Conditions (https://onlinelibrary.wiley.com/terms-and-conditions) on Wiley Online Library for rules of use; OA articles are governed by the applicable Creative Commons License

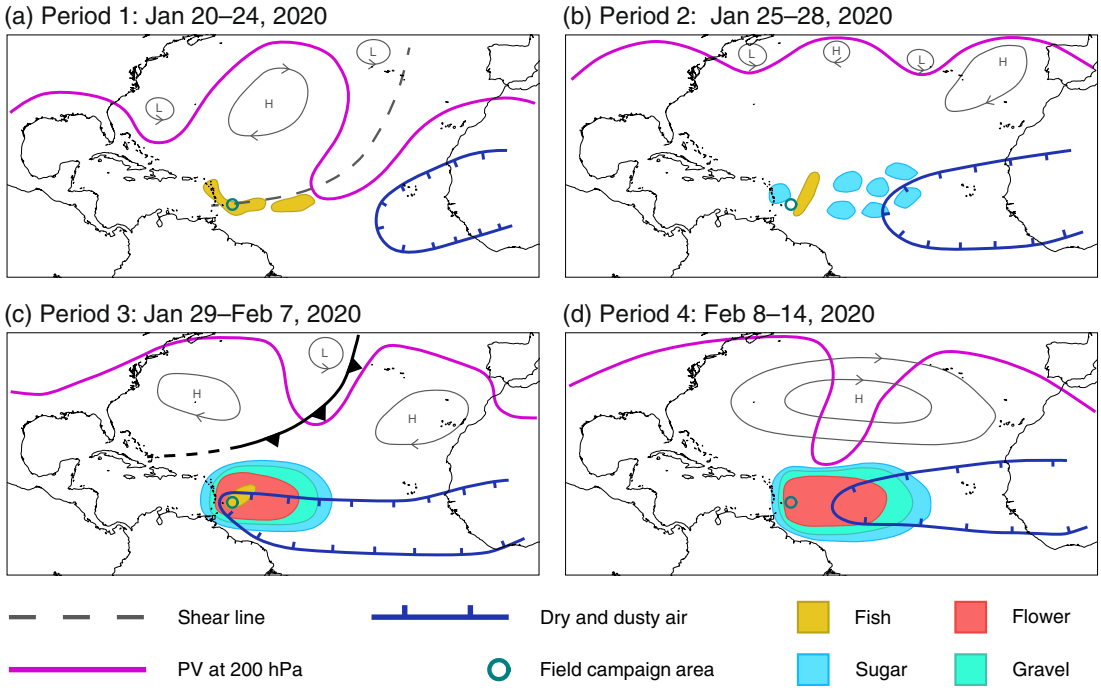


FIGURE 10 Synoptic overview over the EUREC^{4}A field campaign period. Each panel shows the main synoptic features during each of the four periods. Note, the weather features are transient and only the strongest synoptic features at a particular point in time are depicted here. The dominant cloud types in the vicinity of the campaign area (dark blue circle) are encircled. Overlapping cloud-type areas indicate that several cloud types were present during the period. PV: potential vorticity.

5 | CONCLUSIONS AND DISCUSSION

In this article we have examined the large-scale circulation and synoptic-scale features seen during the EUREC^{4}A field campaign and how they relate to observed variations in cloud patterns. This article presents the results of workshops that brought together forecasters and researchers to analyse in detail the synoptic conditions during the field campaign and how they vary.

The results shown here are consistent with Bony *et al.* (2020) finding that differences in low-level wind speed and inversion strength were related to differences in cloud patterns. Subtle differences in low-level winds and the strength of the temperature inversions, as well as low-level moisture, were well linked to differences in clouds and cloud patterns. What we offer here in complement to Bony *et al.* (2020) is to show how the variability of wind and thermodynamic drivers of cloud structure occurs as part of coherent synoptic-scale variability.

At the larger scale, we found that the influence of, or lack of, features associated with the midlatitudes and Subtropics played an important role in the variation of cloud patterns throughout the EUREC^{4}A field campaign period. We identified three features with a notable impact during the field campaign:

1. *The strength and position of subtropical high-pressure systems*. This can be seen in the contrast between the quieter period (January 25–28) when the high pressure is weaker and pushed over North Africa/south Europe, giving a weak pressure gradient and weaker and more zonal winds over the area of interest. Following this a new high-pressure system moved into the North Atlantic and later merged with a second high-pressure system, leading to a strong pressure gradient and stronger and slightly more northerly winds over the area of interest and was associated with more frequent cloud development.
2. *Fronts and shear lines associated with midlatitude cyclones*. The front associated with a cyclone was the dominant feature in the early period (January 20–24), leading to the area of interest being dominated by the fish cloud pattern. Similarly, later in the field campaign, a front advanced south over the Caribbean and led to a similar fish-type cloud pattern but remained north of the region of interest.
3. *Upper-level PV streamers associated with anticyclonic Rossby-wave breaking*. This can also been seen as a change in direction of the subtropical jet, but PV shows a more coherent picture. Generally, the development of deeper clouds and the flowers and gravel patterns in the region was associated with a PV streamer stretching

1477870x, 0, Downloaded from https://rmets.onlinelibrary.wiley.com/doi/10.1002/qj.70311 by Karlsruher Institut Fur Technologie, Wiley Online Library on [10/11/2026]. See the Terms and Conditions (https://onlinelibrary.wiley.com/terms-and-conditions) on Wiley Online Library for rules of use; OA articles are governed by the applicable Creative Commons License

toward the Caribbean. This is consistent with Aemisegger *et al.* (2021) finding that Rossby-wave breaking and its location are important for the transport of extratropical air masses into the Subtropics and the subsequent cloud development.

These features are also not independent. For example, the stronger influence of the subtropical high-pressure systems from January 29 lead to stronger trade winds in the region and was associated with more frequent development of flowers and gravel cloud patterns, consistent with Bony *et al.* (2020). However, the development of deeper clouds was intermittent and more closely associated with the PV streamers. The stronger high pressure is associated with the increased wave activity in the midlatitudes and, therefore, also the PV streamers. The fish cloud pattern is associated with a front/shear line, but there is also a related upper-level trough. In this case the influence of the front/shear line dominates the cloud pattern; but other times, without a front, it is the upper level influence that is more important.

When analysing the strength of the mean local Hadley circulation during the field campaign period, we saw that there was a widespread region of subsidence across the Atlantic and Caribbean (Figure 7a). The anomalies in meridional mass flux, however, showed that the area around Barbados was characterised by reduced ascent (Figure 7b), indicating more favourable conditions for the formation of clouds. We know that the synoptic conditions during these four weeks are not the same. Individual snapshots of the meridional mass flux during each period show that the day-to-day variability of upward and downward mass flux is high (Figure 8). During the earlier part of the EUREC^{4}A period the influence of the high-pressure system was weak, but in period 3, when the anticyclone was located across the whole Atlantic, there was weak ascent on its southern flank, where the field campaign region was located. In period 4, there is widespread weak subsidence across the Atlantic.

Schulz *et al.* (2021) showed that the occurrence of the fish cloud pattern is associated with convergence from extratropical intrusions. This is true in the composite sense and consistent with the early period where the whole region is dominated by the fish cloud pattern; however, there are also plenty of fish-type cloud patterns that form in more typical conditions in the later periods of the field campaign. Though there are regions of fish cloud patterns, they also do not dominate the region like in the early period. This is consistent with Schulz *et al.* (2021) finding that 60% of identified fish cloud patterns have a clear convergence signature. The cases from the EUREC^{4}A field campaign suggest that the remaining cases without a clear convergence signature would be smaller scale and associated with different synoptic conditions, although they may still be related to convergence at those smaller scales.

There were two periods of increased aerosol in Barbados during the field campaign (Chazette *et al.*, 2022; Prospero *et al.*, 2021). Both periods can be associated with an expanding plume of aerosol coming from West Africa. The amount of dust transported across the Atlantic depends on the dust and other aerosols emitted over West Africa and the location of the subtropical anticyclone. The dust events during the EUREC^{4}A field campaign were not extreme, but there were two periods with increased dust emission and transport across the Atlantic. The first dust plume showed some interesting cloud development along the boundary of the airmass as it approached the Caribbean. This detail is likely not picked up by methods of identifying cloud patterns by drawing boxes. It is difficult to say whether the dust had any impact on the cloud development along the boundaries of the airmasses, but it would make an interesting case study for the formation of these clouds.

In summary, we have linked the wider synoptic situation during EUREC^{4}A to the observed cloud patterns. Our analysis and interpretation has brought together the knowledge, expertise, and insight from a community of operational forecasters and scientific researchers. Understanding climate change in these cloud-radiative patterns is not just a question of the cloud-boundary-layer physics but will involve a response to regional circulation and its variability. We need to understand how local processes control the cloud and also how the distribution of cloud on the ocean-basin scale is controlled by these coherent synoptic drivers. Ultimately, we hope that this understanding of the relationships between synoptic drivers and local-scale clouds will assist both in atmospheric modelling and in operational forecasting.

AFFILIATIONS

[1]Department of Meteorology, University of Reading, Reading, UK

[2]Institute for Climate and Atmospheric Science, University of Leeds, Leeds, UK

[3]National Centre for Atmospheric Science, University of Reading, Reading, UK

[4]Met Office, Exeter, UK

[5]CMO, Port of Spain, Trinidad and Tobago

[6]Caribbean Institute for Meteorology and Hydrology, Bridgetown, Barbados

[7]Guyana Hydrometeorological Service, Georgetown, Guyana

[8]Guyana Civil Aviation Authority, Georgetown, Guyana

[9]Grenada Meteorological Service, St George's, Grenada

[10]Antigua and Barbuda Meteorological Service, St John's, Antigua and Barbuda

1477870x, 0, Downloaded from https://rmets.onlinelibrary.wiley.com/doi/10.1002/qj.70311 by Karlsruher Institut Fur Technologie, Wiley Online Library on [10/11/2026]. See the Terms and Conditions (https://onlinelibrary.wiley.com/terms-and-conditions) on Wiley Online Library for rules of use; OA articles are governed by the applicable Creative Commons License

[11]Meteorological Service of Jamaica, Kingston, Jamaica
[12]Météo-France Guadeloupe, Les Abymes, France
[13]Météo-France Guyane, Matoury, French Guiana
[14]St Vincent and the Grenadines Meteorological Service, Kingstown, Saint Vincent and the Grenadines
[15]St Kitts Meteorological Service, Basseterre, Saint Kitts and Nevis
[16]Cayman Islands National Weather Service, George Town, Cayman Islands
[17]Meteorological Department of Sint Maarten, Simpson Bay, Sint Maarten
[18]Barbados Meteorological Service, Bridgetown, Barbados
[19]Trinidad and Tobago Meteorological Service, Piarco, Trinidad and Tobago
[20]The Bahamas Department of Meteorology, Nassau, The Bahamas
[21]Bermuda Weather Service, St George's, Bermuda
[22]National Meteorological Service of Belize, Ladyville, Belize
[23]Danish Meteorological Institute, Copenhagen, Denmark
[24]NORCE Norwegian Research Centre AS, Bergen, Norway
[25]School of Mathematics, University of Leeds, Leeds, UK
[26]National Centre for Atmospheric Science, University of Leeds, Leeds, UK
[27]Centre for Atmospheric Science, Department of Earth and Environmental Sciences, University of Manchester, Manchester, UK
[28]Institute of Meteorology and Climate Research, Karlsruhe Institute for Technology, Karlsruhe, Germany

ACKNOWLEDGMENTS

The workshops and forecast testbed were organised by the University of Leeds and the Caribbean Meteorological Organization (CMO) Headquarters Unit. The Caribbean Institute for Meteorology and Hydrology, the technical and training organ of the CMO, also supported the World Meteorological Organization (WMO) Severe Weather Forecasting Programme-(SWFP)-Eastern Caribbean, which co-sponsored the workshops. CMO's component of the workshops was supported by the WMO and the Climate Risk and Early Warning Systems initiative. The UK component of EUREC^{4}A was funded by the project EUREC^{4}A-UK; NE/S015752/1 (Leeds) and NE/S015779/1 (Manchester). We acknowledge the work of Peter Gallimore, whose early analysis of the atmospheric composition data and vision for a synoptic synthesis encouraged us to develop this article. We thank the three anonymous reviewers whose comments have helped to substantially improve this article.

DATA AVAILABILITY STATEMENT

The data for Figure 2a were taken from the C^{3}ONTEXT dataset (Schulz, 2022). The data from the Barbados Cloud Observatory are freely available online (Stevens *et al.*, 2016). The aerosol data from Figure 2b are available on request. The reanalysis data are from ERA5 (Hersbach *et al.*, 2020), which is freely downloadable from the Climate Data Store (Copernicus Climate Change Service, 2018). The additional aerosol data are from MERRA-2 (Gelaro *et al.*, 2017), which is freely downloadable from the NASA data centre (Global Modeling And Assimilation Office and Pawson, 2015). The satellite images were produced using data from the GOES-16 satellite (Knapp, 2017) downloaded using the GOES-2-go library (Blaylock, 2025). The observed radiosonde soundings were obtained from the University of Wyoming upper air database (Wyoming, 2015). The code used to produce the figures and copies of the synoptic charts are archived in a zenodo repository (Saffin, 2026).

ORCID

Leo Saffin https://orcid.org/0000-0002-6744-7785
Richard Jones https://orcid.org/0000-0002-2777-5805
Leif Denby https://orcid.org/0000-0002-7611-9222
Douglas J. Parker https://orcid.org/0000-0003-2335-8198
Alan Blyth https://orcid.org/0000-0001-7115-2587
Alexander G. Jong https://orcid.org/0009-0000-6412-8749

REFERENCES

Aemisegger, F., Vogel, R., Graf, P., Dahinden, F., Villiger, L., Jansen, F. et al. (2021) How Rossby wave breaking modulates the water cycle in the North Atlantic trade wind region. *Weather and Climate Dynamics*, 2, 281–309. Available from: https://wcd.copernicus.org/articles/2/281/2021/

Beucher, F., Couvreux, F., Bouniol, D., Faure, G., Favot, F., Dauhut, T. et al. (2022) Process-oriented evaluation of the oversea AROME configuration: focus on the representation of cloud organisation. *Quarterly Journal of the Royal Meteorological Society*, 148, 3429–3447.

Blaylock, B.K. (2025) GOES-2-go: Download and display GOES-East and GOES-West data. https://zenodo.org/doi/10.5281/zenodo.4567558

Bony, S. & Dufresne, J.-L. (2005) Marine boundary layer clouds at the heart of tropical cloud feedback uncertainties in climate models. *Geophysical Research Letters*, 32.

Bony, S., Stevens, B., Ament, F., Bigorre, S., Chazette, P., Crewell, S. et al. (2017) EUREC^{4}A: a field campaign to elucidate the couplings between clouds, convection and circulation. *Surveys in Geophysics*, 38, 1529–1568.

Bony, S., Schulz, H., Vial, J. & Stevens, B. (2020) Sugar, gravel, fish and flowers: dependence of mesoscale patterns of trade-wind clouds on environmental conditions. *Geophysical Research Letters*, 48, 2019GL085988.

Bretherton, C.S. & Blossey, P.N. (2017) Understanding mesoscale aggregation of shallow cumulus convection using large-eddy simulation. *Journal of Advances in Modeling Earth Systems*, 9, 2798–2821.

C3S. (2018) ERA5 hourly data on single levels from 1940 to present. https://cds.climate.copernicus.eu/doi/10.24381/cds.adbb2d47

1477870x, 0, Downloaded from https://rmets.onlinelibrary.wiley.com/doi/10.1002/qj.70311 by Karlsruher Institut Fur Technologie, Wiley Online Library on [10/11/2026]. See the Terms and Conditions (https://onlinelibrary.wiley.com/terms-and-conditions) on Wiley Online Library for rules of use; OA articles are governed by the applicable Creative Commons License

Chazette, P., Baron, A. & Flamant, C. (2022) Mesoscale spatio-temporal variability of airborne lidar-derived aerosol properties in the Barbados region during EUREC^{4}A. *Atmospheric Chemistry and Physics*, 22, 1271–1292. Available from: https://acp.copernicus.org/articles/22/1271/2022/

EUREC^{4}A Community (2026) https://howto.eurec4a.eu/bco_cloudradar.html#retrieving-cloud-fraction-profile.

Copernicus Climate Change Service. (2018) ERA5 hourly data on pressure levels from 1940 to present. https://cds.climate.copernicus.eu/doi/10.24381/cds.bd0915c6

Cuevas-Agulló, E., Barriopedro, D., Delia García, R., Alonso-Pérez, S., González-Alemán, J.J., Werner, E. et al. (2024) Sharp increase in Saharan dust intrusions over the western Euro-Mediterranean in February-march 2020-2022 and associated atmospheric circulation. *Atmospheric Chemistry and Physics*, 24, 4083–4104. Available from: https://acp.copernicus.org/articles/24/4083/2024/

Denby, L. (2020) Discovering the importance of mesoscale cloud organization through unsupervised classification. *Geophysical Research Letters*, 47, e2019GL085190.

Gelaro, R., McCarty, W., Suárez, M.J., Todling, R., Molod, A., Takacs, L. et al. (2017) The modern-era retrospective analysis for research and applications, version 2 (MERRA-2). *Journal of Climate*, 30, 5419–5454.

George, G., Stevens, B., Bony, S., Klingebiel, M. & Vogel, R. (2021) Observed impact of mesoscale vertical motion on cloudiness. *Journal of the Atmospheric Sciences*, 78, 2413–2427.

George, G., Stevens, B., Bony, S., Vogel, R. & Naumann, A.K. (2023) Widespread shallow mesoscale circulations observed in the trades. *Nature Geoscience*, 16, 584–589. Available from: https://doi.org/10.1038/s41561-023-01215-1

Global Modeling And Assimilation Office &Pawson, S. (2015) MERRA-2 inst3_2d_gas_nx: 2d,3-Hourly,Instantaneous,Single-Level,Assimilation,Aerosol Optical Depth Analysis V5.12.4. https://disc.gsfc.nasa.gov/datacollection/M2I3NXGAS_5.12.4.html

Gutleben, M., Groß, S., Heske, C. & Wirth, M. (2022) Wintertime Saharan dust transport towards the Caribbean: an airborne lidar case study during EUREC^{4}A. *Atmospheric Chemistry and Physics*, 22, 7319–7330. Available from: https://acp.copernicus.org/articles/22/7319/2022/

Hersbach, H., Bell, B., Berrisford, P., Hirahara, S., Horányi, A., Muñoz-Sabater, J. et al. (2020) The ERA5 global reanalysis. *Quarterly Journal of the Royal Meteorological Society*, 146, 1999–2049.

Janssens, M., de Arellano, J.V., Scheffer, M., Antonissen, C., Siebesma, A.P. & Glassmeier, F. (2021) Cloud patterns in the trades have four interpretable dimensions. *Geophysical Research Letters*, 48, e2020GL091001.

Janssens, M., de Arellano, J.V.-G., van Heerwaarden, C.C., de Roode, S.R., Siebesma, A.P. & Glassmeier, F. (2022) Non-precipitating shallow cumulus convection is intrinsically unstable to length-scale growth. *Journal of the Atmospheric Sciences*, 80, 1–870.

Knapp, K.R. (2017) Gridded Satellite GOES Coverage Data (GridSat-GOES).

Lafore, J.P., Chapelon, N., Beucher, F., Kane, M.D., Gaymard, A., Kasimou, A. et al. (2017) West African synthetic analysis and forecast. In: *Meteorology of tropical West Africa*, John Wiley & Sons, Ltd, pp. 423–451. Available from: https://doi.org/10.1002/9781118391297.ch11

Miller, S.D., Lindsey, D.T., Seaman, C.J. & Solbrig, J.E. (2020) GeoColor: a blending technique for satellite imagery. *Journal of Atmospheric and Oceanic Technology*, 37, 429–448.

Narenpitak, P., Kazil, J., Yamaguchi, T., Quinn, P. & Feingold, G. (2021) From sugar to flowers: a transition of shallow cumulus organization during atomic. *Journal of Advances in Modeling Earth Systems*, 13, e2021MS002619.

Pfahler, M., Bosart, L. & Laing, A. (2025) The role of the subtropical jet stream in dry season severe Caribbean rainstorms: Climatology & Composite Analyses. *Monthly Weather Review*, 153, 111–129. Available from: https://journals.ametsoc.org/view/journals/mwre/aop/MWR-D-23-0264.1/MWR-D-23-0264.1.xml

Prospero, J.M., Delany, A.C., Delany, A.C. & Carlson, T.N. (2021) The discovery of African dust transport to the Western hemisphere and the Saharan air layer: a history. *Bulletin of the American Meteorological Society*. URL https://journals.ametsoc.org/view/journals/bams/102/6/BAMS-D-19-0309.1.xml, 102, E1239–E1260.

Saffin, L. (2026) leosaffin/eurec4a-synoptic: 1st Revision. https://zenodo.org/records/20830278

Saffin, L., Lock, A., Tomassini, L., Blyth, A., Böing, S., Denby, L. et al. (2023) Kilometer-scale simulations of trade-wind cumulus capture processes of mesoscale organization. *Journal of Advances in Modeling Earth Systems*, 15, e2022MS003295. Available from: https://doi.org/10.1029/2022MS003295

Santurette, P. & Joly, A. (2002) ANASYG/PRESYG, Météo-France's new graphical summary of the synoptic situation. *Meteorological Applications*, 9, 129–154. Available from: https://doi.org/10.1017/S1350482702002013

Schulz, H. (2022) C3ONTEXT: a common consensus on convective OrgaNizaTion during the EUREC^{4}A eXperimenT. *Earth System Science Data*, 14, 1233–1256.

Schulz, H., Eastman, R. & Stevens, B. (2021) Characterization and evolution of organized shallow convection in the downstream north atlantic trades. *Journal of Geophysical Research: Atmospheres*, 126, e2021JD034575.

Schwendike, J., Govekar, P., Reeder, M.J., Wardle, R., Berry, G.J. & Jakob, C. (2014) Local partitioning of the overturning circulation in the tropics and the connection to the Hadley and Walker circulations. *Journal of Geophysical Research – Atmospheres*, 119, 1322–1339.

Stevens, B., Farrell, D., Hirsch, L., Jansen, F., Nuijens, L., Serikov, I. et al. (2016) The Barbados cloud observatory: anchoring investigations of clouds and circulation on the edge of the ITCZ. *Bulletin of the American Meteorological Society*, 97, 787–801.

Stevens, B., Bony, S., Brogniez, H., Hentgen, L., Hohenegger, C., Kiemle, C. et al. (2020) Sugar, gravel, fish and flowers: mesoscale cloud patterns in the trade winds. *Quarterly Journal of the Royal Meteorological Society*, 146, 141–152.

Stevens, B., Bony, S., Farrell, D., Ament, F., Blyth, A., Fairall, C. et al. (2021) EUREC^{4}A. *Earth System Science Data*, 13, 4067–4119.

Vial, J., Dufresne, J.-L. & Bony, S. (2013) On the interpretation of inter-model spread in CMIP5 climate sensitivity estimates. *Climate Dynamics*, 41, 3339–3362. Available from: https://doi.org/10.1007/s00382-013-1725-9

Villiger, L., Wernli, H., Boettcher, M., Hagen, M. & Aemisegger, F. (2022) Lagrangian formation pathways of moist anomalies in the

1477870x, 0, Downloaded from https://rmets.onlinelibrary.wiley.com/doi/10.1002/qj.70311 by Karlsruher Institut Fur Technologie, Wiley Online Library on [10/11/2026]. See the Terms and Conditions (https://onlinelibrary.wiley.com/terms-and-conditions) on Wiley Online Library for rules of use; OA articles are governed by the applicable Creative Commons License

trade-wind region during the dry season: two case studies from EUREC^{4}A. *Weather and Climate Dynamics*, 3, 59–88. Available from: https://wcd.copernicus.org/articles/3/59/2022/

Vogel, R., Albright, A.L., Vial, J., George, G., Stevens, B. & Bony, S. (2022) Strong cloud-circulation coupling explains weak trade cumulus feedback. *Nature*, 612, 696–700. Available from: https://doi.org/10.1038/s41586-022-05364-y

Wyoming. (2015) Department atmospheric science university of of wyoming. (2014) worldwide upper air radiosonde soundings, maps, and profiles, by region, 1973-present. Available from: https://weather.uwyo.edu/upperair/sounding.shtml

Zelinka, M.D., Myers, T.A., McCoy, D.T., Po-Chedley, S., Caldwell, P.M., Ceppi, P. et al. (2020) Causes of higher climate sensitivity in CMIP6 models. *Geophysical Research Letters*, 47, e2019GL085782. Available from: https://doi.org/10.1029/2019GL085782

How to cite this article: Saffin, L., Jones, R., Schwendike, J., Laing, A., Caesar, K.-A., Alves, L. *et al*. (2026) A synoptic overview of the EUREC^{4}A field campaign. *Quarterly Journal of the Royal Meteorological Society*, e70311. Available from: https://doi.org/10.1002/qj.70311

1477870x, 0, Downloaded from https://rmets.onlinelibrary.wiley.com/doi/10.1002/qj.70311 by Karlsruher Institut Fur Technologie, Wiley Online Library on [10/11/2026]. See the Terms and Conditions (https://onlinelibrary.wiley.com/terms-and-conditions) on Wiley Online Library for rules of use; OA articles are governed by the applicable Creative Commons License